# Modelling, Simulating and Parameter Designing for Traction Power System with Bidirectional Converter Devices

Jian Zhang [1], Wei Liu [1*], Zhongbei Tian [2], Hao Zhang[1], Jiaxin Zeng[1], He Qi[1]

[1] School of Electrical Engineering, Southwest Jiaotong University, Chengdu, China
[2] Department of Electrical Engineering and Electronics, University of Liverpool, Liverpool, U.K.
[*]liuwei_8208@swjtu.cn

**Abstract: The bidirectional converter device (BCD) can substitute the substation rectifier and the energy feedback system (EFS) by transforming energy between the AC side and DC side. However, the performance of the railway system with BCDs as only converters has not been fully understood. A simulation approach is required to evaluate the system performance and guide the design. In this paper, the traction power supply system considering the capacity constraint of BCDs is modelled first, and the AC/DC power calculating algorithm is studied. A three-layer double-loop parameter designing strategy based on the enhanced brute force (EBF) is proposed, which considers the N-1 principle. In the case study, the power source model for trains and power constraint for BCDs are verified. The boundary configuration set is obtained. The capacity of BCDs is at least 7MW, while the slope is 0 and the no-load voltage is between 1730V and 1750V. Finally, compared with the system with rectifiers and EFSs, the system with BCDs has better performance, which is 46.7V less of the rail potential, 127.8V less of network voltage fluctuation, and 735.56kWh per hour more of the feedback energy.**

## 1. Introduction

In urban rail transit, trains brake frequently due to the short distance between stations, and trains usually adopt regenerative braking to avoid wasting energy. Fig 1 (a) shows the traditional diode rectifier unit. Research on how to take full advantage of regenerative braking energy (RBE) has been studied [1]. At present, the technologies which are applied widely are the energy feedback system (EFS) and the energy storage system (ESS) [2-3]. The energy is transferred from the DC to the AC side through the EFS, supplying energy for AC step-down loads, as in Fig 1(b); the ESS realizes the efficient utilization of RBE by storing and releasing energy at the DC side, as in Fig 1 (c) [4-5]. In recent years, the research on the BCD is becoming more and more attractive. The BCD can transform energy between the AC and the DC side, which achieves the function of the rectifier and the EFS at the same time. A BCD based substation requires less space than a rectified and EFS based substation. Besides, its DC voltage-current output characteristics are controllable, which are preferable to the operation of the traction power supply system. The substation with the diode rectifier in parallel with a BCD in Fig.1 (d) is usually adopted recently. In this paper, the BCD based substation, in which all the trains' required energies are powered by BCD, will be discussed, like in Fig.1 (e). In China, the most commonly used DC voltage level is 1500V, and the most commonly used AC voltage level is 35kV or 10kV.

To design the parameters of BCD, the accurate simulation of system performance is a must, where the power flow calculation algorithm will be employed. In the study of high-voltage DC network, the inverter is usually modelled as a voltage source converter (VSC), and the VSC-HVDC model and Newton-Raphson method are used in the AC/DC power flow calculation [6-8]. However, trains are moving loads and the DC railway power system topologies change

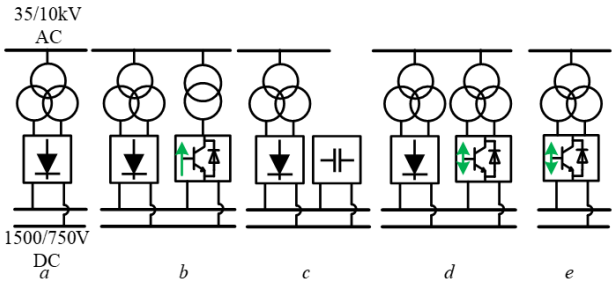


***Fig. 1.*** *The structures of the traction converter* ***(a)*** A traditional diode type substation, ***(b)*** A substation with the diode rectifier in parallel with an EFS, ***(c)*** A substation with the diode rectifier in parallel with an ESS, ***(d)*** A substation with the diode rectifier in parallel with a BCD, ***(e)*** A BCD based substation

dynamically. When it comes to urban rail transit, the detailed drive model of trains is proposed to calculate energy consumption. However, the traction substation (TS) model is not detailed [9]. In [10], different types of TSs, including the TS with BCD are modelled, but only DC power flow is calculated in the algorithm. A new idea of AC/DC unified power flow calculation is proposed, which adopts a new technique based on graph theory to model the motion of the trains in [11], but the system model does not contain the BCD model. Since the BCD and the EFS share almost the same diagram structure, the algorithm of the EFS can be as the reference. The slope rate of EFS is optimized considering economic factors in [12] using the power flow calculator in [13]. The linearization of the DC power flow equations is proposed in [14], and the BCD is also mentioned, but the modelling is simplified. The DC voltage-current output characteristic of the BCD considering the power constraint is proposed in [15], but it mainly focuses on transient-state and steady-state models rather than the power flow calculation model. The algorithm with BCD is proposed and the case is

studied, but the capacity constraint is not taken into account [18].

As for the parameter designing, in [16], the capacity of EFS is determined by the Genetic Algorithm (GA). In [18], the DC voltage control scheme based on the optimal power flow is proposed, and the structure is as Fig.1 (d). When adopting this structure, the capacity of the BCD is not quite vital, because the rectifier can share traction power peak. The design theory of the power supply system of the BCD is in its infancy. In [18], the capacity designing results are given, but the power constraint of BCDs' characteristics needs to be improved. The enhanced brute force (EBF), GA-PSO (particle swarm optimization) algorithm is applied in train trajectory optimization, which can be the reference in parameter designing [19][20].

In reality, the capacity of the BCD, i.e., its rated power, is limited nowadays, due to the low overloading capacity of IGBT. For example, an IGBT of 4 MW can only allow 4 MW peak power, while a 4 MW rectifier can reach 3 times continuous overload in one minute. What is more, the cost of BCD is much higher than the rectifier. Some other parameters like no-load voltage and the slope (the ratio of voltage to current when the BCD works in rated power) of the DC voltage-current output characteristic will also affect system performance, so its parameter designing is quite vital when designing the traction power supply system in urban rail. The previous researches main focus on the device performance of the BCD and its control theories, the parameter designing has not been fully studied. The main contributions of this paper can be summarized as follows:

1) When modelling the BCD, the power constraint in the DC voltage-current output characteristic is considered. When modelling trains, the power source model is taken into account. The power supply system model is built in detail, which includes AC nodes, and other DC nodes. The AC/DC power flow calculating algorithm based on the mentioned models is proposed.

2) A three-layer double-loop parameter designing strategy based on enhanced brute force (EBF) is proposed. In the outer loop, it designs the capacity and slope of the BCD; in the inner loop, it designs the no-load voltage of the BCD.

3) This paper verifies that the power source modelling of trains gives more accurate results than the current source modelling.

4) The power constraint in the DC voltage-current output characteristic of the BCD is verified. The parameter designing results are analyzed, which is more accurate than the results in [18]. The advantages of the BCD based TSs are analyzed compared to traditional TSs with the rectifier paralleled with the EFS based on the parameter designing results.

This paper is organized as follows: Section 2 introduces the modelling of trains and network nodes in the traction power supply system. Section 3 discusses the DC voltage-current output characteristics of BCD and the corresponding models. In Section 4 and 5, the AC/DC power flow calculation algorithm and the parameter designing strategy are proposed. In Section 6, a typical subway case is studied. The algorithm is verified first for the power source model of trains and the power constraint of the BCD. Then the designing results are shown and the system with the rectifier and the EFS is compared with the system with the BCD in system performance including the rail potential (RP), traction network voltage (TNV), and feedback energy.

## 2. Power Supply System Model in Urban Rail

The model of the power supply system should be constructed accurately and completely to provide the base of the power flow calculation. In this section, the structure of the power supply system in urban rail transit is analyzed first, and the models of trains, DC nodes, and AC nodes are built. As for the BCD, its model will be built separately in the next section.

In the power supply system of urban rail transit, the main substations are connected to the power network and transform 110kV AC to 35kV AC. The medium voltage cables connect the main substations, traction substations, and step-down substations. In traction substations, BCDs convert energy between the 35kV AC and the 1500V DC side. Trains get traction energy from the DC traction network, which is connected to the positive side of traction substations, which is the positive DC bus in Fig 2. The traction current flows back to the negative side of traction substations through the rail.

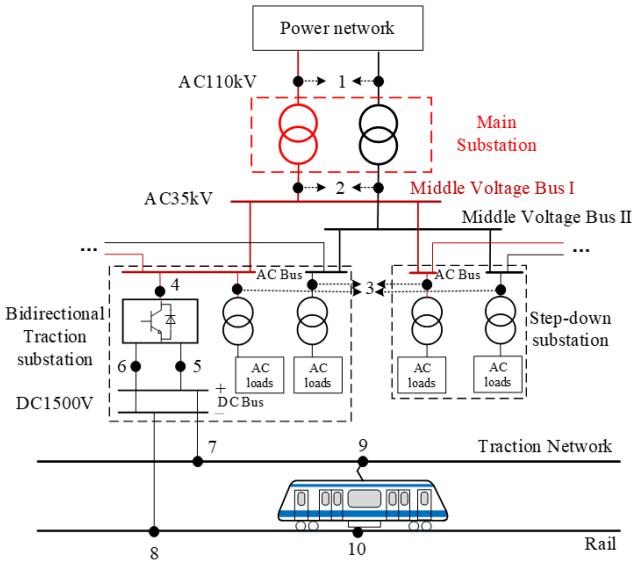


***Fig. 2.*** *The structure and nodes of the power supply system in urban rail transit*

The structure and nodes of the power supply system in urban rail transit are shown in Fig 2, where nodes 1 and 2 represent the high-voltage side nodes and low voltage side nodes of the main transformers. Nodes 3 represents the step-down load nodes. Nodes 4 represents the AC side nodes of the BCDs. Nodes 5 and 6 represent the positive side nodes and negative side nodes of the BCD. Nodes 7 and 8 represent the traction network nodes and rail nodes. Nodes 9 and 10 represent the positive train nodes and negative train nodes.

### *2.1. Trains*

Trains are usually modelled as the current source or power source. The current or power of the train is fixed each simulation time step, which can be obtained by field test or traction calculation. The train models are shown in Fig 3, in which $U_{tpi}$ and $U_{tni}$ are the voltage at the positive node and negative node of the train; $P_{ti}$ is the power between $t_{pi}$ and $t_{ni}$.

$I_{ti}$ is DC current flowing out of $t_{pi}$ and into $t_{ni}$. The node $t_{pi}$ and $t_{ni}$ correspond to the node 9 and 10 in Fig 1.

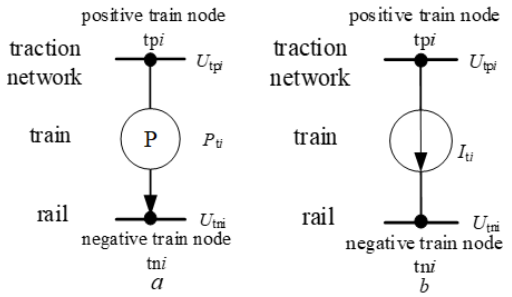


***Fig. 3.*** *The train models*
***(a)*** Power source model, ***(b)***Current source model

When the train is modelled as the power source, the $P_{ti}$ is known, while $U_{tpi}$ and $U_{tni}$ are unknown. According to power balance, the power deviation equations of tp*i* and tn*i* are

$$\begin{cases} \Delta P_{tpi} = P_{ti} + (U_{tpi} - U_{tni}) \sum_{m=1}^{M} G_{tpi,m} U_m \\ \Delta P_{tni} = P_{ti} - (U_{tpi} - U_{tni}) \sum_{m=1}^{M} G_{tni,m} U_m \end{cases} \quad (1)$$

Where, $U_m$ is the voltage of DC node *m*; $G_{tpi,\,m}$ is the conductance between the node tp*i* and *m*; $G_{tni,\,m}$ is the conductance between the node tn*i* and *m*; *M* is the number of DC nodes.

When the train is modelled as the current source, the $I_{ti}$ is known. According to KCL, the current deviation equations of tp*i* and tn*i* are

$$\begin{cases} \Delta I_{tpi} = I_{di} - \sum_{m=1}^{M} G_{tpi,m} U_m \\ \Delta I_{tni} = I_{di} + \sum_{m=1}^{M} G_{tni,m} U_m \end{cases} \quad (2)$$

Define $\Delta\mathbf{P_{tp}}$ as $\{\Delta P_{tp1}, \Delta P_{tp2}, \ldots, \Delta P_{tpTN}\}$, in which *TN* is the number of trains. Similarly, $\Delta\mathbf{P_{tn}}$, $\Delta\mathbf{I_{tp}}$, and $\Delta\mathbf{I_{tn}}$ can be obtained.

For all the positive and negative train nodes, their deviation equations form the deviation vector of trains, $\Delta\mathbf{P_{tp}}$ and $\Delta\mathbf{P_{tn}}$ or $\Delta\mathbf{I_{tp}}$ and $\Delta\mathbf{I_{tn}}$, which will be used in the later power flow calculation.

### *2.2. AC Nodes and DC nodes*

Nodes 1, 2, and 3 in Fig 1 can be classified into AC nodes, and the power deviation equations of an AC node, a*i* are

$$\begin{cases} \Delta P_{ai} = P_{ai} - \sum_{n=1}^{N} U_{ai} U_n \left( G_{ai,n} \cos\theta_{ai,n} + B_{ai,n} \sin\theta_{ai,n} \right) \\ \Delta Q_{ai} = Q_{ai} - \sum_{n=1}^{N} U_{ai} U_n \left( G_{ai,n} \sin\theta_{ai,n} - B_{ai,n} \cos\theta_{ai,n} \right) \end{cases} \quad (3)$$

Where, $P_{ai}$ and $Q_{ai}$ are the power flowing into a*i*; $U_{ai}$ is the voltage amplitude of a*i*; $U_n$ is the voltage amplitude of AC node *n*; $G_{ai,n}$ and $B_{ai,n}$ are real and imaginary parts of the admittance matrix between a*i* and *n*; $\theta_{ai,n}$ is phase angle difference between a*i* and *n*; *N* is the number of AC nodes.

Nodes 7 and 8 in Fig. 1. can be classified into DC nodes, and the deviation equation of a DC node, d*i* is:

$$\Delta P_{di} = P_{di} - \sum_{m=1}^{M} U_{di} U_m G_{di,m} \quad (4)$$

Where, $P_{di}$ is the active power flowing into d*i*; $U_{di}$ is the voltage of d*i*; $G_{di,m}$ is the conductance between d*i* and DC node *m*.

Define $\Delta\mathbf{P_a}$ as $\{\Delta P_{a1}, \Delta P_{a2}, \ldots, \Delta P_{aN}\}$. Similarly, $\Delta\mathbf{Q_a}$ and $\Delta\mathbf{P_d}$ can be obtained, which will be used in the later power flow calculation.

## 3. Bidirectional Converter Device

Except for the modelling of trains, AC nodes, and DC nodes, the modelling of traction substation is also significant. In the BCD based traction substation, the BCD connects the AC side and the DC side of the traction power supply system. Its structure is shown in Fig. 4.

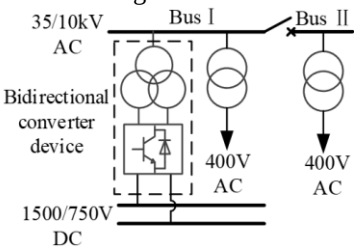


***Fig. 4.*** *The structure of BCD based traction substation*

The BCD is composed of the isolation transformer and the four-quadrant converter bridges and the electric reactors. It is a four-quadrant converter with controllable output voltage [21]. A sample main circuit diagram is shown in Fig. 5, which is the three-level structure. In it, two converter bridges are in parallel. In addition to that, the two-level structure is also widely applied [22].

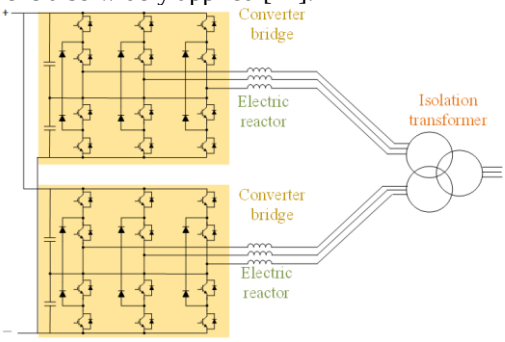


***Fig. 5.*** *A sample main circuit diagram*

### *3.1. DC voltage-current Output Characteristics of the BCD*

The DC voltage-current output characteristics of the BCD at the DC side are shown in Fig.6. In the figure, when the BCD is in the inverter mode, the current is negative at the DC side.

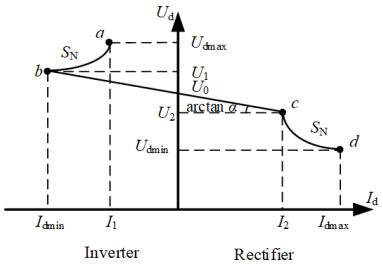


***Fig. 6.*** *The DC voltage-current output characteristics of the BCD at the DC side*

Where $U_d$ and $I_d$ are the voltage and current at the DC side; $U_0$ is the no-load voltage; $I_{dmax}$ and $I_{dmin}$ are the limit values of current during rectifier and inverter modes; $U_{dmax}$ and $U_{dmin}$ are the limit values of voltage during rectifier and inverter modes. The rated capacity of the BCD is $S_N$. $U_1$ and $U_2$ are the voltage at the turning points between the *bc* section and the *ab* or the *cd* section. At point *a*, BCD is inverting at rated power, and the $U_d$ reaches $U_{dmax}$, which means that much surplus regenerated power needs to be absorbed in the traction network near the TS. At point *d*, BCD is rectifying at rated power, and the $U_d$ reaches $U_{dmin}$, which means that many trains required traction power near the TS. The point *b*/*c* is the turning point from drooping DC voltage-current output characteristic to constant power voltage-current output characteristic.

The DC voltage-current output characteristic of the BCD at the *bc* section can be expressed by (5), and the output characteristic of BCD at the *ab* or *cd* section is (6).

$$U_d = U_0 - \frac{U_0 - U_2}{I_2} I_d = U_0 + \frac{U_0 - U_1}{I_{dmin}} I_d \tag{5}$$

$$S_N = U_{dmin} \cdot I_{dmax} = U_2 \cdot I_2 = -U_1 \cdot I_{dmin} = -U_{dmax} \cdot I_1 \tag{6}$$

Set $\alpha$ as the slope of the DC voltage-current output characteristic curve, which is as (7). In Fig. 6., the phase between line *bc* and the *x*-axis is arctan $\alpha$.

$$\alpha = \frac{U_0 - U_2}{I_2} \tag{7}$$

When $\alpha$=0, the output voltage is stable; when $\alpha$>0, the DC voltage-current output characteristic is drooping. The drooping characteristic can be realized by a load current feedforward method or a weakened voltage control loop method.

### 3.2. The Modelling of the BCD

The equivalent circuit of the BCD consists of equivalent impedances and four-quadrant converters, as shown in Fig. 7. The AC voltage of the BCD is $U_s\angle\theta_s$, and $U_s$ is the rms value; the valve side voltage of the four-quadrant converter is $U_c\angle\theta_c$, and $U_c$ is the rms value. The power is $P_s+jQ_s$. The equivalent impedance is $Z_s=R_s+jX_s$, including the impedance of the isolating transformer and the filter reactor.

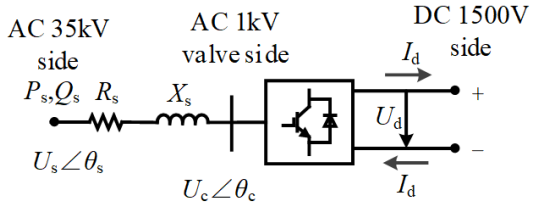


***Fig. 7.*** *The equivalent circuit of the BCD*

According to VSC converter modelling, $U_d = \sqrt{2}U_c/(\mu_s m_s)$. $\mu_s$ is the DC voltage utilization, which is the ratio of the VSC output phase voltage amplitude of the fundamental frequency component to DC voltage, and $\mu_s \in (0,1]$. When the modulation method is SVPWM, $\mu_s$ is 1. $m_s$ is the modulation degree, which is the ratio of modulation amplitude peak to carrier peak, and $m_s \in [0,1]$ [8]. They are both related to the output power of the BCD. By changing the phase difference $\delta_s$ (the difference of $\theta_s$ and $\theta_c$) and $m_s$, the magnitude and direction of the active power and reactive power of the four-quadrant converter can be controlled, achieving bidirectional flow of energy.

The power supply calculation equations for the BCD node *j* are [18]:

$$\begin{aligned} P_{sj} &= -\left(\mu_{sj} m_{sj}/\sqrt{2}\right) U_{sj} U_{dj} Y_{sj} \cos\left(\delta_{sj} + \alpha_{sj}\right) \\ &\quad + U_{sj}^2 Y_{sj} \cos\alpha_{sj} \\ Q_{sj} &= -\left(\mu_{sj} m_{sj}/\sqrt{2}\right) U_{sj} U_{dj} Y_{sj} \sin\left(\delta_{sj} + \alpha_{sj}\right) \\ &\quad + U_{sj}^2 Y_{sj} \sin\alpha_{sj} \\ U_{dj} I_{dj} &= \left(\mu_{sj} m_{sj}/\sqrt{2}\right) U_{sj} U_{dj} Y_{sj} \cos\left(\delta_{sj} - \alpha_{sj}\right) \\ &\quad - \left(\mu_{sj} m_{sj}/\sqrt{2}\right)^2 U_{dj}^2 Y_{sj} \cos\alpha_{sj} \end{aligned} \tag{8}$$

In which, $\delta_{sj}=\theta_{sj}-\theta_{cj}$; $Y_{sj}=1/\sqrt{R_{sj}^2+X_{sj}^2}$; $\alpha_{sj}$=arctan ($X_{sj}/R_{sj}$); $P_{sj}$, $Q_{sj}$, $U_{dj}$, $I_{dj}$, $U_{sj}$, $m_{sj}$, $\mu_{sj}$ are the $P_s$, $Q_s$, $U_d$, $I_d$, $U_s$, $m_s$, $\mu_s$ of the BCD node *j*. The equations represent the active power, reactive power that flows to the AC side of the BCD and the power equality between the DC side and the valve side, respectively. The assumptions are: $U_d > \sqrt{2}\,U_s$; the loss of VSC is less than 5% of the capacity of VSC, which determines the value of $R_s$.

According to (8), the deviation equations of the BCD node *j* are:

$$\begin{cases} \Delta P_{sj} = \sum_{n=1}^{N} U_{sj} U_n \left(G_{j,n}\cos\theta_{j,n} + B_{j,n}\sin\theta_{j,n}\right) - P_{sj} \\ \Delta Q_{sj} = \sum_{n=1}^{N} U_{sj} U_n \left(G_{j,n}\sin\theta_{j,n} - B_{j,n}\cos\theta_{j,n}\right) - Q_{sj} \\ \Delta d_{1j} = U_{dj} I_{dj} + \left(m_{sj}/\sqrt{2}\right)^2 U_{dj}^2 Y_{sj}\cos\alpha_{sj} \\ \qquad - \left(m_{sj}/\sqrt{2}\right) U_{sj} U_{dj} Y_{sj} \cos\left(\delta_{sj} - \alpha_{sj}\right) \end{cases} \tag{9}$$

In which, $\mu_{sj}$ is set as 1; $Gj_{,n}$ and $B_{j,n}$ are real and imaginary parts of the admittance matrix between the AC side of the BCD node *j* and the AC side node *n*; $\theta_{j,n}$ is phase angle difference between the node *j* and *n*; $\Delta d_{1j}$ represents the active power balance.

Some other deviation equations need to be added to obtain the unknown parameters ($m_{sj}$ and $\delta_{sj}$). To control TNV and compensate reactive power, $U_d$ and $Q_s$ are chosen as controlled parameters. The added equations for the BCD node *j* are (10), in which $\Delta d_{2j}$ represents the reactive power balance, and the reactive power of the BCDs is set as $Q_{com}$; $\Delta d_{3j}$ represents the DC voltage-current output characteristics of the BCD; when the $I_{dj}$ is in $[I_{dmin}, I_{d2}]$ and the $U_{dj}$ is in $(U_2, U_1)$, $\Delta d_{3j}$ corresponds to the *bc* segment in Fig. 6; when the $U_{dj}$ is in $[U_1, U_{dmax}]$ or $[U_{dmin}, U_2]$, $\Delta d_{3j}$ corresponds to the *ab* or *cd* segment in Fig. 6.

$$\begin{cases} \Delta d_{2j} = Q_{com} - Q_{sj} \\ \Delta d_{3j} = \begin{cases} U_{dj} - (U_0 - \alpha I_{dj}) & (I_{dmin} \le I_{dj} \le I_2 \\ & \quad \& \ U_2 < U_{dj} < U_1) \\ U_{dj} I_{dj} - S_N & (U_{dmin} \le U_{dj} \le U_2 \\ & \quad \text{or } U_1 \le U_{dj} \le U_{dmax}) \end{cases} \end{cases} \tag{10}$$

As for the DC side of the BCD, the positive and negative nodes of the BCD, bp*j* and bn*j* have deviation equations as:

$$\begin{cases} \Delta P_{\mathrm{bp}j} = U_{\mathrm{bp}j} I_{\mathrm{d}j} - \sum_{m=1}^{M} U_{\mathrm{bp}j} U_m G_{\mathrm{bp}j-m} \\ \Delta P_{\mathrm{bn}j} = U_{\mathrm{bn}j} I_{\mathrm{d}j} + \sum_{m=1}^{M} U_{\mathrm{bn}j} U_m G_{\mathrm{bn}j-m} \end{cases} \quad (11)$$

Where $U_{\mathrm{bp}j}$ and $U_{\mathrm{bn}j}$ are the voltage at the bp$j$ and bn$j$; $G_{\mathrm{bp}j\text{-}m}$ is the conductance between the node bp$i$ and the node $m$; $G_{\mathrm{bn}j\text{-}m}$ is the conductance between bn$j$ and $m$. It is worthy to note that the AC node $j$ and the DC node bp$j$ and bn$j$ all refer to the same BCD. And node $j$, bp$j$, and bn$j$ are different from other nodes in type.

All the deviation equations of BCD nodes can form the deviation vector: $\Delta\mathbf{P}_{\mathrm{s}}$, $\Delta\mathbf{Q}_{\mathrm{s}}$, $\Delta\mathbf{d}_1$, $\Delta\mathbf{d}_2$, $\Delta\mathbf{d}_3$, $\Delta\mathbf{P}_{\mathrm{bp}}$, and $\Delta\mathbf{P}_{\mathrm{bn}}$, which will be used in later power flow calculations.

## 4. Power Flow Calculation Algorithm with the BCD

The modelling of all components in the power supply system provides the condition for the power flow calculation. Based on the Newton-Rapson algorithm, the power flow calculation algorithm is proposed, and its summary is shown in **Alg. 1**. It needs configuration parameters of the trains ($\mathbf{p}_{\mathbf{trains}}$), configuration parameters of the lines ($\mathbf{p}_{\mathbf{lines}}$), configuration parameters of the operation timetable of trains ($\mathbf{p}_{\mathbf{ot}}$), configuration parameters of the substations ($\mathbf{p}_{\mathbf{subs}}$), configuration parameters of the links (including cables, traction network, and rails, etc.) ($\mathbf{p}_{\mathbf{links}}$). The iteration error is $\varepsilon$, and the maximum iteration is $k_{\max}$. The parameters including node voltage, node current ($\mathbf{v}_{\mathbf{n}}$, $\mathbf{i}_{\mathbf{n}}$) will be the output values.

---

**Input:** $\mathbf{p}_{\mathbf{subs}}$, $\mathbf{p}_{\mathbf{links}}$, $\mathbf{p}_{\mathbf{lines}}$, $\mathbf{p}_{\mathbf{trains}}$, $\mathbf{p}_{\mathbf{ot}}$, $\varepsilon$, $k_{\max}$
**Output:** $\mathbf{v}_{\mathbf{n}}$, $\mathbf{i}_{\mathbf{n}}$

1. **COMPUTE** $T = f(\mathbf{p}_{\mathbf{ot}})$ ←Total simulation time
2. **SET** $t = 1$ ← Simulation time
3. **COMPUTE** $\mathbf{G} = f(\mathbf{p}_{\mathbf{subs}}, \mathbf{p}_{\mathbf{links}})$ ← AC side admittance matrix
4. **SET** $k$=1, **all** $\mathbf{v}_{\mathbf{n}}(k) = 1$, $\mathbf{m}_{\mathbf{s}}(k)$=1, $\boldsymbol{\delta}_{\mathbf{s}}(k) = 0$← Parameters init.
5. **COMPUTE** $\mathbf{i}_{\mathbf{n}}(k) = f(\mathbf{p}_{\mathbf{trains}}, \mathbf{p}_{\mathbf{subs}})$
6. **COMPUTE** $\mathbf{Y} = f(\mathbf{p}_{\mathbf{trains}}, \mathbf{p}_{\mathbf{lines}}, \mathbf{p}_{\mathbf{ot}}, t)$ ← DC side admittance matrix
7. **COMPUTE** $\mathbf{F}(k) = f(\mathbf{v}_{\mathbf{n}}(k), \mathbf{i}_{\mathbf{n}}(k), \mathbf{m}_{\mathbf{s}}(k), \boldsymbol{\delta}_{\mathbf{s}}(k), \mathbf{G}, \mathbf{Y})$
8. **IF** $\max(\mathbf{F}(k)) < \varepsilon$ or $k \geqslant k_{\max}$ **GOTO 14**
9. **COMPUTE** $\mathbf{J}(k)$
10. $\Delta\mathbf{X}(k) = \mathbf{J}(k)^{-1} \bullet \mathbf{F}(k)$
11. $k = k + 1$
12. **COMPUTE** $\mathbf{v}_{\mathbf{n}}(k)$, $\mathbf{i}_{\mathbf{n}}(k)$, $\mathbf{m}_{\mathbf{s}}(k)$, $\boldsymbol{\delta}_{\mathbf{s}}(k) = f(\mathbf{v}_{\mathbf{n}}(k\text{-}1), \mathbf{i}_{\mathbf{n}}(k\text{-}1), \mathbf{m}_{\mathbf{s}}(k\text{-}1), \boldsymbol{\delta}_{\mathbf{s}}(k\text{-}1), \Delta\mathbf{X}(k\text{-}1))$
13. **COMPUTE** $\mathbf{F}(k) = f(\mathbf{v}_{\mathbf{n}}(k), \mathbf{i}_{\mathbf{n}}(k), \mathbf{m}_{\mathbf{s}}(k), \boldsymbol{\delta}_{\mathbf{s}}(k), \mathbf{G}, \mathbf{Y})$ **GOTO 8**
14. $t = t + 1$
15. **IF** $t \leq T$ **GOTO 4**
16. **ELSE** *Break*

---

***Algorithm 1:*** *Summary of power flow calculation algorithm with BCD*

First, the total simulation time ($T$) is obtained through the train operation timetable ($\mathbf{p}_{\mathbf{ot}}$). Then, the simulation time ($t$) is initialized as 1. At step 3, the AC side admittance matrix $\mathbf{G}$ can be attained by parameters of the links ($\mathbf{p}_{\mathbf{links}}$), and it is constant throughout the simulation. Step 4~13 describes the simulation snapshot at time $t$. In step 14~16, $t$ increases 1 first, for the time step in this paper is 1 second. If $t$ exceeds T, the simulation ends and the results are output; else the simulation snapshot at time $t$ will be executed.

In the simulation snapshot at time $t$, there are mainly two parts: the preparation and first calculation, which corresponds to step 4~8; the iteration, which corresponds to step 8~13.

In the first part, the number of iterations, $k$, is initialized to 1; the node voltage at $k$th iteration, $\mathbf{v}_{\mathbf{n}}(k)$ is initialized to 1; the $m_{\mathrm{s}}$ at $k$th iteration, $\mathbf{m}_{\mathbf{s}}(k)$ is initialized to 1; the $\delta_{\mathrm{s}}$ at $k$th iteration, $\boldsymbol{\delta}_{\mathbf{s}}(k)$ is initialized to 1. At step 5, the node current at $k$th iteration, $\mathbf{i}_{\mathbf{n}}(k)$ is calculated by $\mathbf{p}_{\mathbf{trains}}$ and $\mathbf{p}_{\mathbf{subs}}$. Then the DC side admittance matrix ($\mathbf{Y}$) is calculated according to $\mathbf{p}_{\mathbf{trains}}$, $\mathbf{p}_{\mathbf{lines}}$, $\mathbf{p}_{\mathbf{ot}}$, and $t$. In step 7, According to section II and III, the deviation vector at $k$th iteration, $\mathbf{F}(k)$ is established as (12) when trains are modelled as power sources. The" ($k$)" in (12) ~ (14) means the $k$th iteration. When trains are modelled as current sources, $\Delta\mathbf{P}_{\mathbf{tp}}$ and $\Delta\mathbf{P}_{\mathbf{tn}}$ should be replaced by $\Delta\mathbf{I}_{\mathbf{tp}}$ and $\Delta\mathbf{I}_{\mathbf{tn}}$.T stands for the transpose of a vector. At step 8, the maximum absolute value in $\mathbf{F}$, $\max(\mathbf{F})$ is compared with the convergence accuracy, $\varepsilon$. If $\max(\mathbf{F}) < \varepsilon$ or $k$ is equal to or greater than $k_{\max}$, jump to step 14, which means the simulation of $t$ ends.

$$\mathbf{F}(k) = \begin{bmatrix} \Delta\mathbf{P}_{\mathrm{a}}(k) & \Delta\mathbf{Q}_{\mathrm{a}}(k) & \Delta\mathbf{P}_{\mathrm{s}}(k) & \Delta\mathbf{Q}_{\mathrm{s}}(k) \cdots \\ \Delta\mathbf{d}_1(k) & \Delta\mathbf{d}_2(k) & \Delta\mathbf{d}_3(k) & \Delta\mathbf{P}_{\mathrm{bp}}(k) \cdots \\ \Delta\mathbf{P}_{\mathrm{bn}}(k) & \Delta\mathbf{P}_{\mathrm{d}}(k) & \Delta\mathbf{P}_{\mathrm{tp}}(k) & \Delta\mathbf{P}_{\mathrm{tn}}(k) \end{bmatrix}^{\mathrm{T}} \quad (12)$$

In the second part, at step 9 the Jacobian matrix of $k$th iteration, $\mathbf{J}(k)$ is computed. According to (13), the full equation is shown in (14) when trains are modelled as power sources. When trains are modelled as current sources, $\Delta\mathbf{P}_{\mathbf{tp}}$ and $\Delta\mathbf{P}_{\mathbf{tn}}$ should be replaced by $\Delta\mathbf{I}_{\mathbf{tp}}$ and $\Delta\mathbf{I}_{\mathbf{tn}}$, and the elements in the Jacobian matrix should also change. In (14), the quantities denote the deviation vectors of the variables at $k$th iteration. For example, $\mathbf{A}_1(\mathrm{k})$ is the partial derivative of $\Delta\mathbf{P}_{\mathbf{a}}(k)$ to $\Delta\boldsymbol{\theta}_{\mathbf{s}}(k)$.

$$\mathbf{F}(k) = \mathbf{J}(k) \cdot \Delta\mathbf{X}(k) \quad (13)$$

$$\begin{bmatrix} \Delta\mathbf{P}_{\mathrm{a}}(k) \\ \Delta\mathbf{Q}_{\mathrm{a}}(k) \\ \Delta\mathbf{P}_{\mathrm{s}}(k) \\ \Delta\mathbf{Q}_{\mathrm{s}}(k) \\ \Delta\mathbf{d}_1(k) \\ \Delta\mathbf{d}_2(k) \\ \Delta\mathbf{d}_3(k) \\ \Delta\mathbf{P}_{\mathrm{bp}}(k) \\ \Delta\mathbf{P}_{\mathrm{bn}}(k) \\ \Delta\mathbf{P}_{\mathrm{d}}(k) \\ \Delta\mathbf{P}_{\mathrm{tp}}(k) \\ \Delta\mathbf{P}_{\mathrm{tn}}(k) \end{bmatrix} = \begin{bmatrix} \mathbf{A}_1(k) & \mathbf{A}_2(k) & \mathbf{A}_3(k) & \mathbf{A}_4(k) & & & & & & & & \\ \mathbf{B}_1(k) & \mathbf{B}_2(k) & \mathbf{B}_3(k) & \mathbf{B}_4(k) & & & & & & & & \\ \mathbf{C}_1(k) & \mathbf{C}_2(k) & \mathbf{C}_3(k) & \mathbf{C}_4(k) & & \mathbf{C}_6(k) & \mathbf{C}_7(k) & \mathbf{C}_8(k) & \mathbf{C}_9(k) & & & \\ \mathbf{D}_1(k) & \mathbf{D}_2(k) & \mathbf{D}_3(k) & \mathbf{D}_4(k) & & \mathbf{D}_6(k) & \mathbf{D}_7(k) & \mathbf{D}_8(k) & \mathbf{D}_9(k) & & & \\ & & \mathbf{E}_3(k) & \mathbf{E}_4(k) & \mathbf{E}_5(k) & \mathbf{E}_6(k) & \mathbf{E}_7(k) & \mathbf{E}_8(k) & \mathbf{E}_9(k) & & & \\ & & & & \mathbf{F}_5(k) & & & \mathbf{F}_8(k) & \mathbf{F}_9(k) & & & \\ & & & \mathbf{G}_4(k) & & \mathbf{G}_6(k) & \mathbf{G}_7(k) & \mathbf{G}_8(k) & \mathbf{G}_9(k) & & & \\ & & & & \mathbf{H}_5(k) & & & \mathbf{H}_8(k) & \mathbf{H}_9(k) & \mathbf{H}_{10}(k) & \mathbf{H}_{11}(k) & \mathbf{H}_{12}(k) \\ & & & & \mathbf{I}_5(k) & & & \mathbf{I}_8(k) & \mathbf{I}_9(k) & \mathbf{I}_{10}(k) & \mathbf{I}_{11}(k) & \mathbf{I}_{12}(k) \\ & & & & & & & \mathbf{G}_8(k) & \mathbf{G}_9(k) & \mathbf{G}_{10}(k) & \mathbf{G}_{11}(k) & \mathbf{G}_{12}(k) \\ & & & & & & & \mathbf{H}_8(k) & \mathbf{H}_9(k) & \mathbf{H}_{10}(k) & \mathbf{H}_{11}(k) & \mathbf{H}_{12}(k) \\ & & & & & & & \mathbf{J}_8(k) & \mathbf{J}_9(k) & \mathbf{J}_{10}(k) & \mathbf{J}_{11}(k) & \mathbf{J}_{12}(k) \end{bmatrix} \begin{bmatrix} \Delta\boldsymbol{\theta}_{\mathrm{a}}(k) \\ \Delta\mathbf{U}_{\mathrm{a}}(k) \\ \Delta\boldsymbol{\theta}_{\mathrm{s}}(k) \\ \Delta\mathbf{U}_{\mathrm{s}}(k) \\ \Delta\mathbf{I}_{\mathrm{d}}(k) \\ \Delta\boldsymbol{\delta}_{\mathrm{s}}(k) \\ \Delta\mathbf{m}_{\mathrm{s}}(k) \\ \Delta\mathbf{U}_{\mathrm{bp}}(k) \\ \Delta\mathbf{U}_{\mathrm{bn}}(k) \\ \Delta\mathbf{U}_{\mathrm{d}}(k) \\ \Delta\mathbf{U}_{\mathrm{tp}}(k) \\ \Delta\mathbf{U}_{\mathrm{tn}}(k) \end{bmatrix} \quad (14)$$

Then the correction vector $\Delta\mathbf{X}(k)$ is calculated as $\mathbf{J}(k)^{-1} \bullet \mathbf{F}(k)$ according to (13) and is shown in (15). At step 11, $k$ increases by 1. Then according to $\Delta\mathbf{X}(k\text{-}1)$, variables including $\mathbf{v}_{\mathbf{n}}(k)$, $\mathbf{i}_{\mathbf{n}}(k)$, $\mathbf{m}_{\mathbf{s}}(k)$ and $\boldsymbol{\delta}_{\mathbf{s}}(k)$ are computed. At step 13, $\mathbf{F}(k)$ is calculated; go to step 8 to judge whether the iteration should end or not.

$$\Delta\mathbf{X}(k) = \begin{bmatrix} \Delta\boldsymbol{\theta}_{\mathrm{a}}(k) & \Delta\mathbf{U}_{\mathrm{a}}(k) & \Delta\boldsymbol{\theta}_{\mathrm{s}}(k) & \Delta\mathbf{U}_{\mathrm{s}}(k) & \Delta\mathbf{I}_{\mathrm{d}}(k) & \Delta\boldsymbol{\delta}_{\mathrm{s}}(k) \cdots \\ \Delta\mathbf{m}_{\mathrm{s}}(k) & \Delta\mathbf{U}_{\mathrm{bp}}(k) & \Delta\mathbf{U}_{\mathrm{bn}}(k) & \Delta\mathbf{U}_{\mathrm{d}}(k) & \Delta\mathbf{U}_{\mathrm{tp}}(k) & \Delta\mathbf{U}_{\mathrm{tn}}(k) \end{bmatrix}^{\mathrm{T}} \quad (15)$$

## 5. Parameter Designing Strategy

Based on the proposed power flow algorithm, a parameter designing strategy is proposed. The "N-1"

principle should be considered, which is that the power supply system should meet the load demand during peak hours when any traction substation is out of operation. The parameters of the BCDs to design include $S_N$, $\alpha$, and $U_0$, because they are closely related to the system performance of urban rail transit. The seeking process is based on the Enhanced Brute Force (EBF), which is a straightforward approach to solve problems in the area of computer science by enumerating all the possibilities in the limited solution domain [23][24], which is different from the Brute Force (BF) algorithm because EBF restricts the feasible region.

The structure of the parameter designing is shown in Fig. 8. $\mathbf{p_{lines}}$, $\mathbf{p_{trains}}$, $\mathbf{p_{ot}}$, $\mathbf{p_{links}}$, $\varepsilon$, and $k_{max}$ are fixed input parameters; $\mathbf{p_{subs}}$, including $S_N$, $U_0$, and $\alpha$ need to be adjusted according to the parameter designing strategy. After power flow calculation, the iteration results ($\mathbf{v_n}$, $\mathbf{i_n}$) and the boundary configuration set, which will be discussed later, are output.

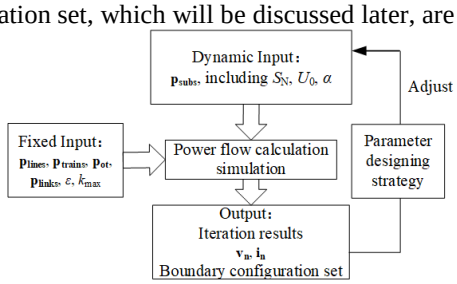


***Fig. 8.*** *The structure of the parameter designing*

According to [18], $S_N$ and $\alpha$ are both closely related to the peak power of BCDs. $U_0$ affects the RP and TNV but has little impact on peak power. Therefore, the parameter designing strategy has a three-layer double-loop structure. The three-layer stands for $S_N$, $\alpha$, and $U_0$. The double-loop stands for the loops of $S_N$ and $\alpha$. For the outer loop, $S_N$ decreases. For the inner loop, $\alpha$ decreases while $S_N$ keeps constant. After that, for the specific $S_N$ and $\alpha$, $U_0$ is sought to meet RP and TNV limitations.

**Step 1: Find the initial capacity, $S^{(0)}$.**

The urban rail traction power supply without considering the capacity constraint of the BCD is simulated and $\alpha$ is set as 0 because in this case, the power peak of BCD is the greatest [18]. Each TS is turned off in turn to follow the "N-1" principle. There is a default $U_0$, such as 1650V. As the result, the maximum value of the peak power of all BCDs is the $S^{(0)}$, and it is the case that TS$n$ is turned off.

**Step 2: Find the feasible $S_N$ and $\alpha$.**

In this step, the iteration of $S_N$ is defined as $k$, and the iteration of $\alpha$ is defined as $x$. The $S_N$ in the $k_{th}$ iteration, $S^{(k)}$, is shown in (16); the $\alpha$ in the $x_{th}$ iteration of $\alpha$ and the $k_{th}$ iteration of $S_N$, $\alpha_{(k)}^{(x)}$, is shown in (17), where the capacity step length is $S_w$; the slope step length is $\alpha_w$; $\alpha^{(0)}$ is the initial slope, and it can be the maximum value which the BCD allows.

$$S^{(k)}=S^{(0)}-kS_w \tag{16}$$

$$\alpha_{(k)}^{(x)}=\alpha^{(0)}-x\alpha_w \tag{17}$$

The solution tracks of BF and EBF in $S_N$ and $\alpha$ dimensions is shown in Fig. 9., in which $i$ is the number in the iteration.

Fig. 9.(a) shows the solution track of BF. Each solution corresponds to a specific $S_N$ and a specific $\alpha$, and it needs to be simulated with each $U_0$ in the feasible region.

Fig. 9.(b) shows the solution track of EBF. When $\alpha$ decreases while $S_N$ keeps constant, the process is inner loop. The inner loop continues until $\alpha$ is 0 or the solution is infeasible, which means there are non-convergent moments in the iteration results. Then move to the next $S^{(k)}$ and do the inner loop again, until there are not any feasible solutions for $S^{(k)}$. There are two aspects that increase simulation efficiency: 1) The solutions which are circled by the blue line in Fig. 9.(b) do not need to be simulated according to the rules of EBF. 2)The solutions which are surrounded by blue in Fig. 9.(b) need to be simulated to find the feasible $U_0$ in the feasible region, while other solutions do not need to be simulated.

The detailed procedure of Step 2 is: first, $k$ and $x$ are initialized as 0. Then the simulation applying the proposed power flow algorithm is carried out with the condition that the TS$n$ is turned off. In the inner loop, the $x$ increases each loop, until $\alpha_{(k)}^{(x)}$ is less than 0 or there are not non-convergence moments in the results. For the former case, $x$ minus 1; go to Step 3. For the latter case, if $x$ is not 0, steps are the same, otherwise, the simulation ends. The purpose of subtracting $x$ by 1 is restoring $x$ which allows the simulation to converge. After Step 3, it will go to the outer loop. $k$ increases by 1 and $x$ is set to 0. And it will go to the simulation again.

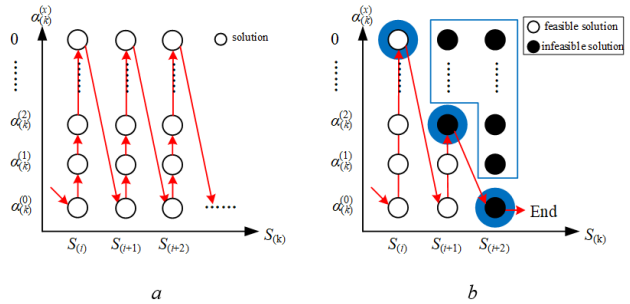


***Fig. 9.*** *The solution tracks of BF and EBF in $S_N$ and $\alpha$ dimensions*
***(a)*** *BF,* ***(b)****EBF*

**Step 3: Find the feasible $U_0$.**

According to [18], $U_0$ is negatively related to RP but positively related to TNV. When adjusting $U_0$, the step length can be 10V, and $U_0$ should be in [1000V, 1800V]. The simulation starts from the default $U_0$ rather than 1000V or 1800V. Then, $U_0$ increases until the RP or TNV does not meet the demand or $U_0$ reaches 1800V. Next, $U_0$ decreases until the RP or TNV does not meet the demand or $U_0$ reaches 1000V. The $U_0$ is recorded in $\{U_0\}$ if the TNV and the RP both meet the limitation. If $\{U_0\}$ is not empty for a certain $\alpha_{(k)}^{(x)}$, then the configuration ($S^{(k)}$, $\alpha_{(k)}^{(x)}$, $\{U_0\}$) can be recorded. Finally, the boundary configuration set is {($S^{(k)}$, $\alpha_{(k)}^{(x)}$ ,max$\{U_0\}$, min$\{U_0\}$)}. The max$\{U_0\}$ is the maximum value in $\{U_0\}$, and min$\{U_0\}$ is the minimum value in $\{U_0\}$.

The parameter designing strategy is shown in Fig. 10.

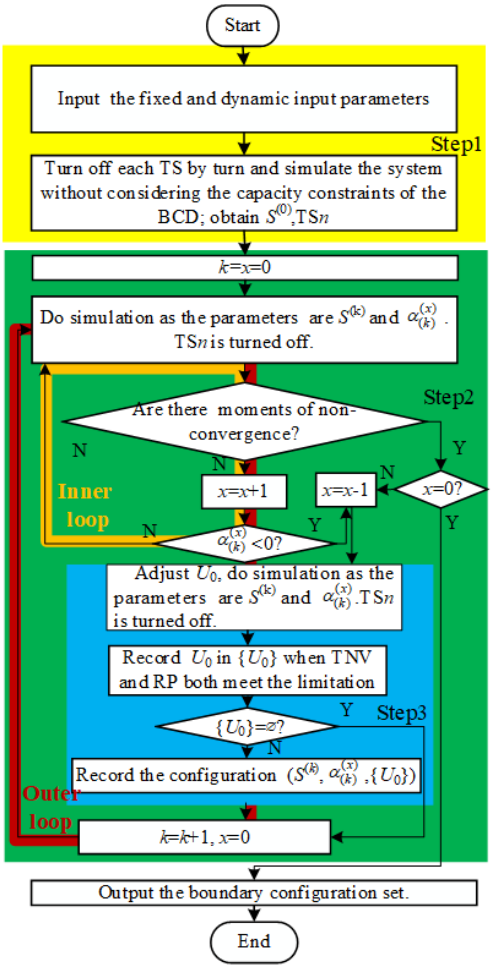


***Fig. 10.*** *The parameter designing strategy*

## 6. Case Study

Xuzhou Metro 2 is studied as the typical example, and its topology is shown in Fig. 11. The power supply system is equipped with two main substations, and 10 traction substations, namely TS1-TS10 and 10 step-down substations. The parameters of the system are shown in TABLE 1. In the table, the load ratio is the ratio of the real step-down load to the install capacity of the step-down transformer. It is worth mentioning that since only the steady-state model is considered in this paper, the reactance of traction net and rail is ignored.

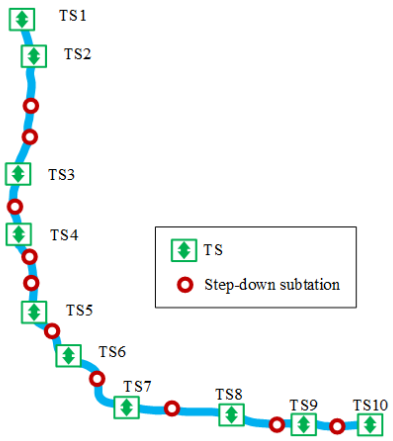


***Fig. 11.*** *The topology of Xuzhou Metro 2*

**Table 1 Parameters of the System**

| | |
|---|---|
| Capacity of main substations | 2*40MVA |
| Resistance of traction network | 0.0173 Ω/km |
| Resistance of rail | 0.02 Ω/km |
| Load ratio of step-down substations | 0.25 |
| Top speed of trains | 80km/h |

In this metro project, route 1 means trains run from TS1 to TS10, while for route 2, trains run only in TS3-TS10 section. The operation timetable for trains is as TABLE 2. For peak hour, the headway time of route 1 is 257s, and the headway time of route 2 is 514s. $\alpha$ = 0, and $\varepsilon = 10^{-6}$.

**Table 2 Parameters of the System**

| Headway time of route 1 (second) | Headway time of route 2 (second) | Operation time (hour) |
|---|---|---|
| 257 | 514 | 2 |
| 300 | 600 | 2 |
| 360 | 720 | 2 |
| 360 | - | 8 |
| 450 | - | 1 |
| 600 | - | 1 |

The train curves are shown in Fig. 12.

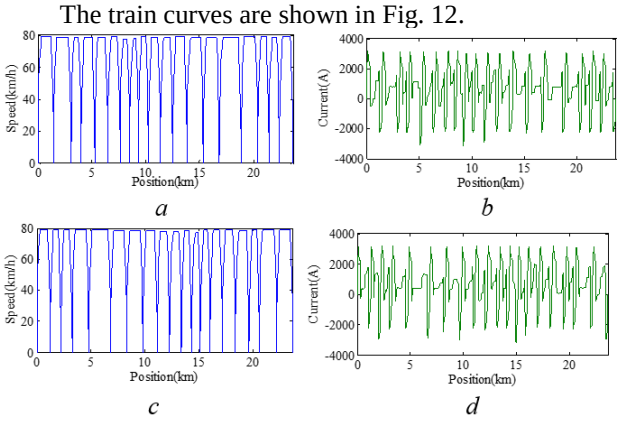


***Fig. 12.*** *The curves of trains*
***(a)***upward position-speed curve, ***(a)*** upward position-current curve, ***(a)***downward position-speed curve, ***(a)*** downward position-current curve

Some cases are designed and their information is shown in TABLE 3, in which ①stands for the headway time of peak hour in TABLE 2, and ② stands for the headway time of route 1 is 120s. For the 6B trains, their weight with rated load is 291.6t. For the 8A trains, their weight with rated load is 462.1t, and their highest speed is 120km/h.

**Table 3 Case information**

| Case | Train model | power constraint of the BCDs | Train Type | Headway time |
|---|---|---|---|---|
| 1 | current source | Not considered | 6B | ① |
| 2 | power source | Not considered | 6B | ① |
| 3 | power source | 8MW | 6B | ① |
| 4 | power source | 5MW | 6B | ① |
| 5 | power source | Considered | 8A | ① |
| 6 | power source | Considered | 6B | ② |

### 6.1. Verification of the power source model of trains

In [18], the power flow calculation algorithm does not consider the capacity constraint, and the trains adopt the current source model.

In Case1, the algorithm in [18] is adopted, which means the trains adopt the current source model; Case2 adopts the algorithm, which means the trains adopt the power source model, while the power constraint of the BCD is not considered.

A specific moment, $t$ = 365s is studied. It is worthy to mention that the current of trains that adopt the current source is the quotient of its power and initial voltage. Fig.13 ~Fig.15 are the results.

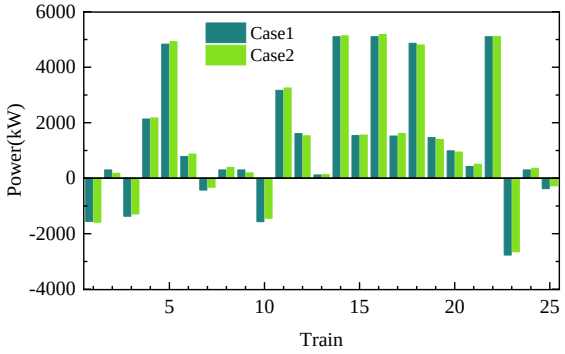


***Fig. 13.*** *The power of trains in different cases*

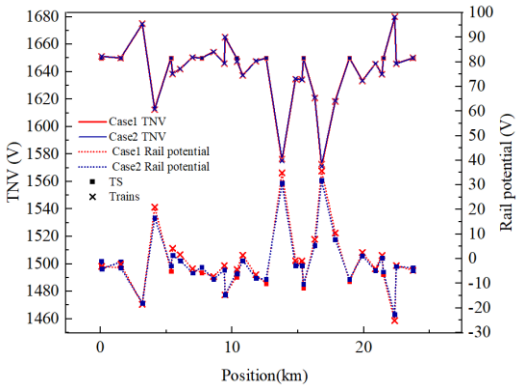


***Fig. 14.*** *The TNV and RP of trains and TSs in different cases*

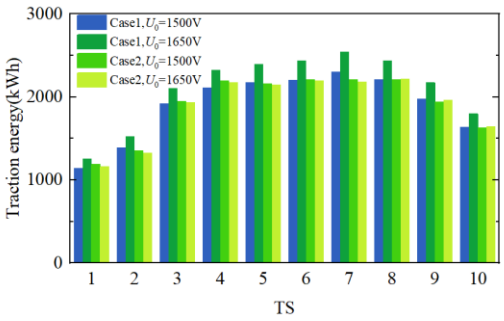


***Fig. 15.*** *The traction energy per hour in different cases and* $U_0$

In Fig. 13, the positive power indicates traction, while the negative power indicates regenerative braking. It can be seen in Fig.13 and Fig.14 that the power difference of the two models is relatively close, with a maximum difference of 147.89kW; the maximum difference of TNV is 0.63V; the maximum difference of the RP is 4.28V.

The traction energy consumption per hour under different $U_0$ is counted in Fig 15, and $U_0$ is set to 1500V and 1650V respectively. When in Case1, the largest change of traction energy is TS7 with the change rate of 10.5%. When in Case2, that is 1.6%. As $U_0$ increases, the system TNV level also rises. When in Case1, the traction power of trains increases, so the traction energy consumption also inclines subsequently. However, $U_0$ has less impact on traction power and energy when in Case2. Therefore, using the power source model can achieve more reliable simulation results than using the current source model.

### 6.2. Verification of the power constraint

To verify the capacity constraint of the proposed algorithm, a second, t=365s is analyzed, for there are many trains that are in traction mode. The results are shown in Fig 16 and Fig 17. The $U_0$ and $\alpha$ are set separately as 1650V and 0.

In Case3, the install capacity of BCDs is 8MW. In Case4, the install capacity is 5MW. Case3 and Case4 both use the proposed algorithm that takes the power constraint of the BCD into account.

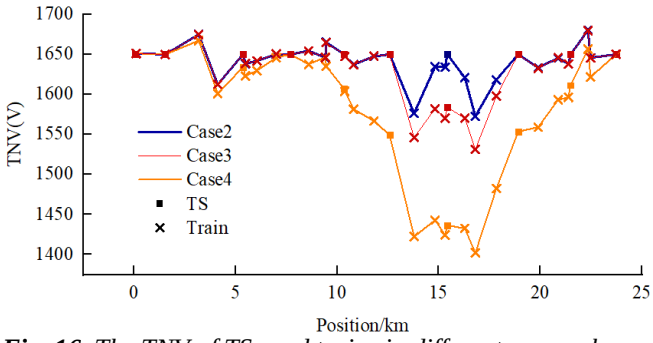


***Fig. 16.*** *The TNV of TSs and trains in different cases when t=365s*

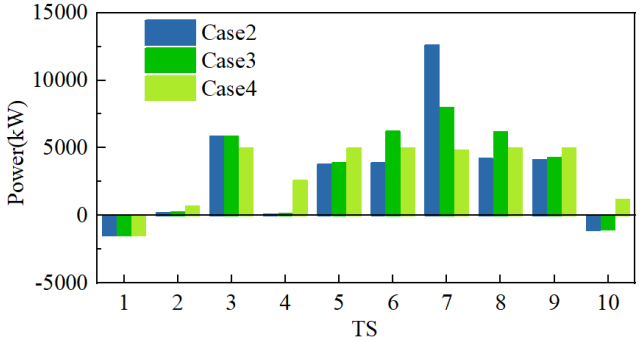


***Fig. 17.*** *The DC power of TSs in different cases when t=365s*

It can be seen from Fig. 16 that the TNV of all TSs in Case2 is 1650V; the TNV of the TS7 in Case3 is 1583.7V and it is 1439.6V in Case5. It can be seen from Fig. 17 that in Case2, the traction power of TS7 is 12.6MW; in Case3, it is limited to 8MW; in Case4, it is limited to 5MW. According to Fig. 6, the DC voltage-current output characteristic of the BCD in TS7 is in the *cd* segment in Case3 and Case4. The decline of TNV at TS7 also lowered the TNV of nearby trains and make the power support from other TSs possible. In

Case3, TS6 and TS8 provide power support for TS7, while in Case4, TS4-TS10 provide power support for TS7, and their power is 5MW.

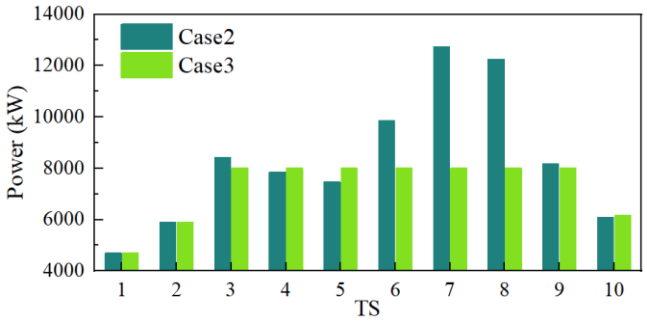


***Fig. 18.*** *The DC power of TSs in different cases during the simulation process*

From Fig.18, it is obvious that the peak power of TS3~9 is restricted to 8MW in all seconds of the simulation in Case3. Case4 is not in the figure for there are non-convergent moments in the iteration results.

It is proved that the proposed algorithm in this paper is effective when constraining the peak power of BCDs and the results are reasonable.

### *6.3. Parameter designing of the BCD*

According to the proposed strategy in Section V, the first step is finding $S^{(0)}$. Through simulation, it is known that $S^{(0)}$= 13.4MW and TS7 is turned off. $S_w$ = 0.5MW. $\alpha_w$=0.01Ω.

Based on the TNV and RP constraints, the boundary configuration set of the BCDs is shown in Table 4. The maximum absolute values of the RP under different $U_0$ and $S_N$ are shown in Fig. 19.

**Table 4 The Boundary Configuration Set of the BCDs**

| $S_N$(MW) | $\alpha$(Ω) | max{$U_0$} (V) | min{$U_0$} (V) |
|---|---|---|---|
| 7 | 0 | 1730 | 1750 |
| 7.5 | 0 | 1720 | 1750 |
| 8 | 0 | 1700 | 1750 |
| 8.5 | 0 | 1690 | 1750 |
| 9 | 0 | 1680 | 1750 |
| 9.5 | 0 | 1680 | 1750 |

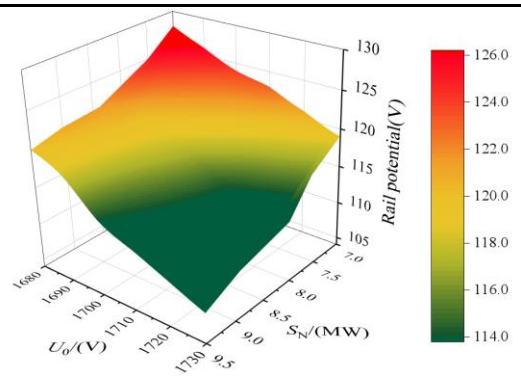


***Fig. 19.*** *The maximum absolute value of the RP under different* $U_0$ *and* $S_N$

If the traditional brute force search algorithm is used, because the feasible region of $S_N$, $\alpha$, and $U_0$ contain 26, 7, and 81 values, it needs 14,742 times of simulation to get all feasible solutions. By using the proposed EBF algorithm, all the solution sets are obtained by 249 times, which is 1.63% of the traditional algorithm.

It can be seen that when $S_N$ or $U_0$ increases, the RP decreases. When $S_N$ increases, the power transmission between TSs decreases, so the RP declines. The reason why the RP decreases as $U_0$ increases is that higher TNV means less current through rail. The maximum RP keeps the same when the capacity constraint is 9.5MW and 10MW. Since the maximum value of the RP is caused by the instantaneous start power requirement of multi traction trains, when the capacity of the BCD is already sufficient to provide the power required for the traction of the train, continuing to increase the capacity of the BCD will not affect the maximum RP. Since the TNV is all in the limit, the figures are not shown.

To research the influence of train speed and operation timetable of trains on the parameter designing result of the BCDs, Case5 and Case6 are also studied, and the results are shown in TABLE 5. Comparing with Case2, when the highest speed of trains is 120km/h (train type: 8A), its minimum $S_N$ increases by 42.9% in Case5; when the headway time of trains is 120s, its minimum $S_N$ increases by 50% in Case6.

**Table 5 The Boundary Configuration Set of the BCDs**

| Case | $S_N$(MW) | $\alpha$(Ω) | max{$U_0$} (V) | min{$U_0$} (V) |
|---|---|---|---|---|
| 5 | 10 | 0 | 1740 | 1750 |
| 6 | 10.5 | 0 | 1730 | 1750 |

### *6.4. Comparisons between different TS schemes*

In this case study, different TS schemes are compared. In Scheme A, the TSs are with the diode rectifier in parallel with the EFS, which has been widely used in metro projects currently. The capacity of the diode rectifiers is 2×3MW, and their no-load voltage is 1664V. The capacity of EFSs is 2MW and their start voltage is 1680V. In Scheme B, the TSs are BCD based TSs. The capacity of BCDs is 7MW according to the boundary configuration set. $U_0$ is set to 1670V, which is between 1664V and 1680V. $\alpha$ is 0. The TNV and RP performance of the two schemes are shown in TABLE 5, and the feedback energy per hour of the two schemes is shown in Fig. 20.

**Table 5 The TNV and RP Performance of Two Schemes**

| Scheme | $U_{rmax}$(V) | $U_{tmax}$(V) | $U_{tmin}$(V) |
|---|---|---|---|
| A | 79.8 | 1793.8 | 1490.2 |
| B | 33.1 | 1746.3 | 1570.5 |

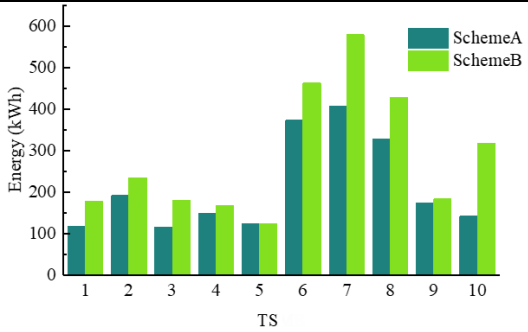


***Fig. 20.*** *The energy per hour of two schemes*

From Table IV, it can be seen that the $U_{rmax}$ in scheme A is 79.8V, which is 46.7V greater than $U_{rmax}$ in Scheme B. The $U_{tmax}$ of Scheme A is 47.5V greater than $U_{tmax}$ of Scheme B, and $U_{tmin}$ of Scheme A is 80.3V less than $U_{tmin}$ of Scheme B. It is indicated that Scheme B has better performance on controlling RP and TNV.

It can be found in Fig. 20 that the feedback energy per hour in each TS of Scheme B is more than that of Scheme A. The maximum difference between the two schemes is 173.0 kWh at TS7, and the total difference is 735.56kWh per hour. The reason is that compared with Scheme B, in Scheme A, there is a voltage range in the output characteristics, which is from the no-load voltage of rectifier to the start voltage of EFS, and neither rectifier nor EFS will operate in this section. This section prompts the energy flow between traction trains and regenerative braking trains through a long distance which will increase the RP and fluctuation of TNV. Therefore, the feedback energy is less, and the RP and fluctuation of TNV rise.

## 7. Conclusion

In this paper, the traction power supply system is modelled, and the capacity constraint of the BCD is considered. The AC/DC power flow algorithm of the traction power supply system with the mentioned model of the BCD is proposed. The EBF algorithm is applied and a parameter strategy with three layers and double loops is designed. A case is studied and here are the conclusions:

1) The application of the power source of trains is more appropriate comparing with the algorithm which adopts the current source model because the energy consumption is more stable when the traction network voltage changes.

2) The power constraint of the BCD is proved at a moment and in the total process. The power peak is significantly and strictly restricted.

3) Through the mentioned parameter designing strategy, a boundary configuration set is attained. The minimum capacity of BCDs is 7MW, and the slope is 0. The no-load voltage can be between 1730V and 1750V.

4) The system with BCD based TSs has advantages in the RP, fluctuation of TNV, and feedback energy over the system with rectifiers and EFSs. They are 46.7V less, 127.8V less and 735.56kWh per hour more correspondingly.

Note that the parameters of the BCDs in the case study are all the same, but in fact, they can be different in the metro project. In our future research, we will pay more attention to the optimization of parameters of the BCDs.

## 8. References


[1] Arturo, G., Roberto, P., Paul, B. : 'Sustainable urban rail systems: strategies and technologies for optimal management of regenerative braking energy', Energy Conversion and Management, 2013, 5, (75), pp 374-388

[2] Mahdiyeh, K., Ahmed, M., Werner, B.: 'Recuperation of regenerative braking energy in electric rail transit systems', IEEE Transactions on Intelligent Transportation Systems, 2019, 8, (20), pp 2831-2847

[3] Mahdiyeh, K., Ahmed, M.: 'Modeling and simulation of a reversible substation for recuperation of regenerative braking energy in rail transit systems', 2019 IEEE Transportation Electrification Conference and Expo (ITEC), Detroit, USA, June 2019, pp. 1-5.

[4] Pablo, A., Peru, B., Urtzi, A.: 'Energy is on board: energy storage and other alternatives in modern light railways', IEEE Electrification Magazine, 2016, 9, (4), pp 30-41

[5] Tuojian, W., Wei. L., Jian, Z., et al.: 'Analysis of wayside energy storage system in dc traction power supply system'. 2019 IEEE Vehicle Power and Propulsion Conference (VPPC), Hanoi, Vietnam, October 2019, pp. 1-6

[6] Luis, M. C., Enrique, A.: 'A unified modeling approach of multi-terminal VSC-HVDC links for dynamic simulations of large-scale power systems', IEEE Transactions on Power Systems, 2016, 11, (31), pp 5051-5060

[7] Enrique, A., Behzad, K., Luis, M. C.: 'A new VSC-HVDC model for power flows using the Newton-Raphson method', in IEEE Transactions on Power Systems, 2013, 8, (28), pp 2602-2612

[8] Alejandro, P., Claudio R. F., H. A., et al.: 'Modeling of VSC-based HVDC systems for a Newton-Raphson OPF algorithm', IEEE Transactions on Power Systems, 2007, 11, (22), pp 1794-1803

[9] Martyn, Z. C., Alasdair, C. R., Mike, B., et al.: 'Modeling electrified transit systems', IEEE Transactions on Vehicular Technology, 2010, 7, (59), pp. 2748-2756

[10] Pablo, A., Bassam, M., Islam, E.: 'DC railway simulation including controllable power electronic and energy storage devices', IEEE Transactions on Power Systems, 2018, 33, (5), pp 5319-5329

[11] Pablo, A., Guzman, D., Manuel, C.: 'Unified AC/DC power flow for traction systems: a new concept', IEEE Transactions on Vehicular Technology, 2012, 61, (6), pp 2421-2430

[12] Gang, Z., Zhongbei, T., Pietro, T., et al.: 'Inverter operating characteristics optimization for DC traction power supply systems', IEEE Transactions on Vehicular Technology, 2019, 4, (68), pp 3400-3410

[13] Zhongbei, T., Paul, W., Ning, Z., et al.: 'System energy optimisation strategies for metros with regeneration', Transp. Res. Part C Emerg. Technol., 2017, 2, (75), pp. 120–135

[14] Alvaro, J. L., Ramon, R. P., A. P. C., et al.: 'Optimizing mass transit systems electrical infrastructure by application of the particle swarm optimization algorithm'. 2019 IEEE Vehicle Power and Propulsion Conference (VPPC), Hanoi, Vietnam, October 2019, pp. 11-15.

[15] Gang, Z., Zhongbei, T., Pietro, T., et al.: 'A new hybrid simulation integrating transient-state and steady-state models for the analysis of reversible DC traction power systems', International Journal of Electrical Power & Energy Systems, 2019, 2 (109), pp. 9-19

[16] Vasilis, A. K., Nikos, D. H.: 'Optimal control of reversible substations and wayside storage devices for voltage stabilization and energy savings in metro railway networks', IEEE Transportation Electrification, 2019, 6, (5), pp 515–523

[17] Fengjie, H., Gang, Z., Jie, C., et al: 'Optimal voltage regulation and power sharing in traction power systems with reversible converters', IEEE Transactions on Power Systems, 2020, 7 (35), pp 2726-2735

[18] Jian, Z., Wei, L., Ruibing, Z., et al.: 'Modeling and analysis of DC traction power supply system based on bidirectional converter device'. 2019 IEEE Vehicle Power and Propulsion Conference (VPPC), Hanoi, Vietnam, October 2019, pp. 21-26

[19] Zhongbei, T., Ning, Z., Stuart, H., at al.: 'SmartDrive: traction energy optimization and applications in rail systems', IEEE Transactions on Intelligent Transportation Systems,2019, 20, (7), pp 2764-2773

[20] Ziqiang, P., Minwu, C., Shaofeng, L., et al.: 'Integrated timetable optimization for minimum total energy consumption of an AC railway system', IEEE Transactions on Vehicular Technology, 2020, 4, (69), pp. 3641-3653

[21] P. Verdelho: 'Voltage type reversible rectifiers control methods in unbalanced and non-sinusoidal conditions', IECON '98. Proceedings of the 24th Annual Conference of the IEEE Industrial Electronics Society (Cat. No.98CH36200), Aachen, Germany, 1998, pp. 479-484

[22] Pedro, V., G. D. M.: 'DC voltage control and stability analysis of PWM-voltage-type reversible rectifiers', IEEE Transactions on Industrial Electronics,1998, 45, (2), pp 263-273

[23] Hossam, F.: 'Accelerating motif finding problem using grid computing with enhanced Brute Force', 2010 The 12th International Conference on Advanced Communication Technology (ICACT), Phoenix Park, 2010, pp. 197-202.

[24] Ning, Z., Clive, R., Stuart, H., et al.: 'A multiple train trajectory optimization to minimize energy consumption and delay', IEEE Transactions on Intelligent Transportation Systems, 2015, 10, (16), pp. 2363-2372